HHS Public Access

Author manuscript

ACS Biomater Sci Eng. Author manuscript; available in PMC 2022 January 31.

Published in final edited form as:

ACS Biomater Sci Eng. 2021 June 14; 7(6): 2723–2733. doi:10.1021/acsbiomaterials.0c01728.

Modeling Airway Dysfunction in Asthma Using Synthetic Mucus Biomaterials

Daniel Song,
Fischell Department of Bioengineering, University of Maryland, College Park, Maryland 20742, United States

Ethan Iverson,
Department of Cell Biology & Molecular Genetics, University of Maryland, College Park, Maryland 20742, United States

Logan Kaler,
Biophysics Program, University of Maryland, College Park, Maryland 20742, United States

Shahed Bader,
Fischell Department of Bioengineering, University of Maryland, College Park, Maryland 20742, United States

Margaret A. Scull,
Department of Cell Biology & Molecular Genetics, University of Maryland, College Park, Maryland 20742, United States

Gregg A. Duncan
Fischell Department of Bioengineering and Biophysics Program, University of Maryland, College Park, Maryland 20742, United States;

Abstract

As asthma worsens, occlusion of airways with mucus significantly contributes to airflow obstruction and reduced lung function. Recent evidence from clinical studies has shown mucus obtained from adults and children with asthma possesses altered mucin composition. However, how these changes alter the functional properties of the mucus gel is not yet fully understood. To study this, we have engineered a synthetic mucus biomaterial to closely mimic the properties of native mucus in health and disease. We demonstrate that this model possesses comparable biophysical and transport properties to native mucus *ex vivo* collected from human subjects and *in vitro* isolated from human airway epithelial (HAE) tissue cultures. We found by systematically varying mucin composition that mucus gel viscoelasticity is enhanced when predominantly

Corresponding Author: **Gregg A. Duncan** – Fischell Department of Bioengineering and Biophysics Program, University of Maryland, College Park, Maryland 20742, United States; gaduncan@umd.edu.

Supporting Information

The Supporting Information is available free of charge at https://pubs.acs.org/doi/10.1021/acsbiomaterials.0c01728.
Effective hydrodynamic diameters and protein contents of MUC5B (BSM) and MUC5AC (PGM) solutions (Figure S1); quantification of MUC5B and MUC5AC staining intensities in unstimulated and IL-13-stimulated BCi-NS1.1 HAE cultures (Figure S2); microrheology of MUC5B-rich and MUC5AC-rich synthetic mucus following NAC treatment (Figure S3) (PDF)

Complete contact information is available at: https://pubs.acs.org/10.1021/acsbiomaterials.0c01728

The authors declare no competing financial interest.

composed of mucin 5AC (MUC5AC), as is observed in asthma. As a result, asthma-like synthetic mucus gels are more slowly transported on the surface of HAE tissue cultures and at a similar rate to native mucus produced by HAE cultures stimulated with type 2 cytokine IL-13, known to contribute to airway inflammation and MUC5AC hypersecretion in asthma. We also discovered that the barrier function of asthma-like synthetic mucus toward influenza A virus was impaired as evidenced by the increased frequency of infection in MUC5AC-rich hydrogel-coated HAE cultures. Together, this work establishes a biomaterial-based approach to understand airway dysfunction in asthma and related muco-obstructive lung diseases.

Graphical Abstract

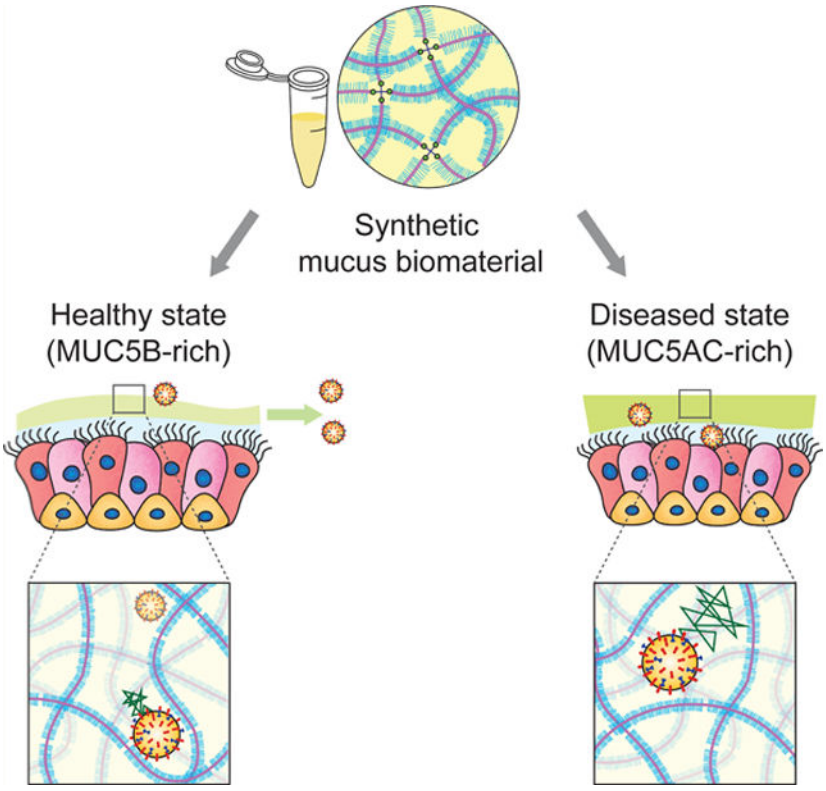

Keywords

respiratory disease; mucus; biomaterials; asthma; influenza

1. INTRODUCTION

Asthma affects ~300 million people worldwide of all racial and ethnic backgrounds with cases documented from childhood to adulthood.[1] As lung disease worsens in asthma, chronic airway inflammation commonly leads to excess production of mucus.[2,3] Mucus is continuously cleared from the lung through high-frequency, coordinated beating of ciliated cells on the surface of the airway epithelium.[4,5] This process, known as mucociliary clearance (MCC), provides the lung with an important defense mechanism against infection

and injury with the continuous removal of inhaled environmental particles captured within the mucus layer.[6] However, in all stages of asthma, MCC mechanisms become impaired, resulting in the accumulation of mucus in the airway.[7] Persistent mucus accumulation not only leads to inflammation and infection by providing an environment for microbial growth but also results in obstruction of conducting airways potentially causing asphyxiation in severe cases of asthma.[8,9] Further, many individuals with asthma suffer from recurrent pulmonary exacerbations characterized as an acute worsening of symptoms requiring emergency department visits and hospitalizations.[10,11] Exacerbations in asthma are often associated with infections by respiratory viruses such as rhinovirus, respiratory syncytial virus (RSV), and influenza.[12–14] Accordingly, it is of importance to understand how the changes in mucus produced in asthma lead to dysfunctional MCC and further examine its potential role in susceptibility to infection.

For effective MCC, the mucus gel must be a soft, shear-thinning, viscoelastic material. The primary building blocks of respiratory mucus are the gel-forming mucins, mucin 5B (MUC5B), and mucin 5AC (MUC5AC).[15] These large (~MDa) and heavily glycosylated proteins form the mucus gel network primarily through reversible associations (e.g., entanglements, hydrogen bonds) and disulfide cross-links. The resulting mesh-like microstructure acts as a selectively permeable barrier that allows passage of certain substances while restricting diffusion of others.[15,16] The assembly of the mucin network gives rise to the viscoelastic properties of mucus, enabling directional transport in response to shear forces exerted by the cilia on the airway surface. Although similar in general structure and amino acid sequence, MUC5B and MUC5AC differ in charge, which is a direct result of differences in their glycosylation patterns. MUC5B is heavily sialylated, whereas MUC5AC has a high fucose content.[3,17] These mucins also possess different amounts and arrangement of hydrophobic and cysteine-containing domains that can further influence hydrogel assembly.[15] Recent evidence has also shown that MUC5B and MUC5AC are capable of forming polymer fibers with distinct morphologies.[3,18]

In individuals with asthma, biochemical analysis of mucus produced by cough has revealed that mucin composition is altered as a function of disease severity, with a shift from MUC5B to MUC5AC as the predominant secreted mucin.[19] Further, computerized tomography (CT) imaging has revealed an increased likelihood and number of mucus plugs within the airway in asthma patients with MUC5AC-enriched airway mucus.[20] These data suggest that overproduction of MUC5AC may predispose the airways to mucus accumulation in asthma. MCC defects in asthma have been attributed to oxidation-induced cross-linking of mucins in the asthmatic lung and physical tethering of MUC5AC to the airway surface,[21–23] both as a result of exaggerated inflammatory responses in asthma. However, it is not yet fully understood how an imbalance in the ratio of MUC5B to MUC5AC contributes to the biological function of mucus in asthma.

Studying airway mucus in health and disease has relied heavily on acquiring *ex vivo* human mucus samples through sputum induction or endotracheal tubes from patients who have undergone intubation.[24,25] However, the limited availability of clinical samples as well as the modest sample volume (~100 μL) using these collection methods presents challenges in mechanistic studies on how altered mucus composition influences its function.

In addition, samples acquired from humans can often possess altered mechanical properties due to sample dilution after sputum induction.[26] These limitations have stimulated interest in synthetic mucus biomaterials that have similar physical properties to airway mucus. Recent studies have reported mucus biomaterials that use commercially available crude mucins, sourced from porcine stomach or bovine submaxillary gland, for studying functional properties, such as rheology and transport.[22,27] In suspension, reconstituted mucins fail to establish covalent bonding and do not form mucin gel networks.[28] Combining mucins with cross-linking agents, such as poly(acrylic) acid (PAA) and thiolated star polyethylene glycol (PEG) polymers, re-establishes covalent cross-linking producing mucin-based biomaterials with *in vivo*-like biophysical properties.[29,30]

In our work, we report a synthetic mucus biomaterial capable of modeling transport and barrier function of airway mucus. Specifically, we have adapted an approach established in our previous work[30] to create disulfide-linked mucin-based hydrogels composed of MUC5B and MUC5AC with viscoelastic properties comparable to airway mucus. This model system provides the capability to systematically vary the composition of mucus to capture how these changes impact its physiological function. Using this model, we examined the rheology of mucin-based hydrogels with a varied and specified MUC5B:MUC5AC ratio to understand the impact of mucin composition on its biophysical properties. Transport of synthetic mucus on fully differentiated human airway epithelial (HAE) tissue cultures was then compared to natively secreted mucus in normal cultures and IL-13-exposed cultures to establish an asthma-like inflammatory condition. To understand the barrier function of synthetic mucus toward respiratory viruses, we directly measured the diffusion of fluorescent IAV within synthetic mucus gels and the extent of infection in synthetic mucus-coated human airway tissue cultures. The results of our work establish a new biomaterial-based approach to create *in vitro* models of asthmatic airways and identify potential mechanisms of lung dysfunction.

2. MATERIALS AND METHODS

2.1. Preparation of Synthetic Mucus.

Synthetic mucus hydrogels were prepared using a previously established method.[30] Briefly, porcine gastric mucin (PGM; Sigma-Aldrich) and mucin from bovine submaxillary glands (BSM; Sigma-Aldrich) were mixed with a cross-linking reagent, 4-arm PEG-thiol (PEG-4SH; Laysan Bio Inc.), to mediate cross-linking between mucin biopolymers. A solution of 4% (w/v) PGM and/or BSM was dissolved in a physiological buffer solution containing 154 mM NaCl, 3 mM $CaCl_2$, and 15 Mm NaH_2PO_4 at pH 7.4 at 4% (w/v) and stirred at room temperature for 2 h. The cross-linking reagent, PEG-4SH, was initially prepared at 4% (w/v) in the same buffer and then mixed with equal volumes of mucin solutions to achieve a final concentration of 2% (w/v) mucin and 2% (w/v) cross-linking reagent. For experiments with varying ratios of MUC5B and MUC5AC, solutions of PGM and BSM were mixed at varying MUC5B:MUC5AC ratios (75:25, 50:50, and 25:75) prior to addition of the cross-linking reagent. The mixed solution of mucin and cross-linker was incubated at room temperature for ≥15 h to allow gelation. For bulk rheology experiments, synthetic mucus hydrogels were prepared in Petri dishes with 40 mm diameter with 2 mm thickness. For PTM experiments, hydrogels were prepared in custom microscopy chambers

prior to gelation. For mucus transport and influenza viral challenge studies, hydrogels were prepared 24 h prior to experiments and UV-disinfected for 15 min before being transferred to HAE tissue cultures.

2.2. Collection of Human Mucus Samples.

Human mucus samples were collected using the endotracheal tube (ETT) method in accordance with an IRB-approved protocol at the University of Maryland Medical Center (Protocol#: HP-00080047). ETTs were collected from patients after intubation as a part of general anesthesia at the UMMC. To collect the ETT-derived *ex vivo* samples, the last 10 cm of the tubes was cut, including the balloon cuff, and suspended in a 50 mL centrifuge tube using a syringe needle. The centrifuge tube containing the ETT was spun at 220*g* for 30 s for mucus collection, which resulted in 100–300 μL of ETT mucus. Samples were stored at −80 °C immediately after collection and thawed (no more than three times) prior to use for experiments.

2.3. Preparation of Nanoparticles for Particle Tracking Microrheology.

Fluorescent carboxylate-modified fluorescent polystyrene nanoparticles (PS-COOH; Life Technologies) with diameters of 100 and 500 nm were coated with high-surface-density polyethylene glycol (PEG) via a carboxyl-amine linkage using 5 kDa methoxy PEG-amine (Creative PEGWorks) as previously reported.[24,30] Particle size and zeta potential were measured in 10 mM NaCl at pH 7 using a NanoBrook Omni (Brookhaven Instruments). We measured diameters of 122 and 491 nm and zeta potentials of −0.54 ± 1.16 and 1.09 ± 0.51 mV for 100 and 500 nm PEG-coated PS nanoparticles, respectively.

2.4. Particle Tracking Microrheology (PTM) Analysis in Human Mucus and Synthetic Mucus.

The diffusion of the PEG-coated nanoparticles (PEG-NP) in human and synthetic mucus gels was measured using fluorescence video microscopy. Mucus samples were prepared in custom microscopy chambers that consisted of O-rings coated in vacuum grease on a microscope slide. Twenty microliters of human mucus was added to the chamber along with 1 μL of ~0.002% w/v suspension of PEG-NP 30 min prior to PTM experiments. Synthetic mucus was prepared by adding 25 μL of mucin and cross-linker solution to the microscopy chamber. 1 μL of ~0.002% w/v suspension of PEG-NP was added to the mucin and cross-linker solution and sealed with a cover slip. Imaging was performed 24 h later after gelation. Fluorescence video microscopy videos were collected using a Zeiss 800 LSM microscope with a 63× water-immersion objective and an Axiocam 702 camera (Zeiss). High-speed videos were recorded at a frame rate of 33 Hz for 10 s at room temperature. For each sample, at least three high-speed videos were recorded. The particle tracking analysis was performed using a previously developed image processing algorithm.[31] Mean squared displacement (MSD) as a function of time lag (τ) was calculated as $\langle \Delta r^2(\tau) \rangle = \langle (x^2 + y^2) \rangle$ for each particle. The pore size of the sample was calculated using $\xi = \sqrt{\mathrm{MSD}_{1s}} + a$, where MSD_{1s} is the measured MSD at $\tau = 1$ s and a is the nanoparticle radius. For *N*-acetylcysteine (NAC) experiments, NAC was added after gelation at a final concentration of 50 mM and incubated for 30 min prior to imaging.

2.5. Measurement of Bulk Rheology.

Dynamic rheological measurements of the synthetic mucus gels were performed using an ARES G2 rheometer (TA Instruments) with a 20 mm diameter parallel plate geometry at 25 °C. To determine the linear viscoelastic region of the fully formed gel, a strain sweep measurement was collected from 0.1 to 10% strain at a frequency of 1 rad/s. To determine the elastic modulus, $G'(\omega)$, and viscous modulus, $G''(\omega)$, a frequency sweep measurement was conducted within the linear viscoelastic region of the gel at 1% strain amplitude and angular frequencies from 0.1 to 100 rad/s.

2.6. Culture of BCi-NS1.1 Cells.

The h-TERT immortalized human airway basal BCi-NS1.1 cell line was generously provided by Dr. Ronald Crystal in which his group established in previous work.[32] Cells were initially seeded on plastic at ~3000 cells/cm^2 in PneumaCult-Ex Plus media (StemCell) and incubated at 37 °C and 5% CO_2. Once cells reached 70–80% confluency, they were dissociated using 0.05% trypsin ethylenediaminetetraacetic acid (EDTA) for 5 min at 37 °C. For differentiation at the air–liquid interface (ALI), cells were seeded on 12 mm diameter Transwell inserts (Corning Costar) coated with 50 μg/mL collagen from human placenta (Sigma Aldrich) at ~10,000 cells/cm^2. An expansion medium, PneumaCult-Ex Plus, was used to feed cells in both the apical and basolateral compartments until 100% confluency. After reaching confluency, the apical medium was removed, introducing the ALI, and the basolateral medium was replaced with PneumaCult-ALI (StemCell). All cells were grown for 28 days to reach differentiation with media exchanged every other day. The collection method for BCi-NS1.1 mucus was adapted from a previously described protocol.[33,34] BCi-NS1.1 mucus was allowed to accumulate for 7 days. *In vitro* mucus samples were harvested by washing apical compartments with PBS for 30 min at 37 °C. After 30 min of incubation, the solution of mucus and PBS in the apical compartment was collected. Samples were loaded into Amicon Ultra 100 kDa filters (Millipore-Sigma) and centrifuged at 14,000*g* for 30 min to remove excess PBS. After filtration, protein concentration was measured using a BCA assay and samples were reconstituted into physiological concentrations (~2 mg/mL)[35] using physiological buffer used to prepare mucin hydrogels. To establish an asthma-like human tissue culture model, BCi-NS1.1 cultures were maintained in a medium with IL-13 (100 ng/mL, Peprotech, Rocky Hill, NJ) for 7 days prior to *en face* staining and MCC experiments.

2.7. Preparation of BCi-NS1.1 Cultures for *En Face* Staining.

For *en face* immunohistochemical staining and fluorescence imaging of MUC5B and MUC5AC, cultures were prepared by aspirating the culture medium from the basolateral compartment and adding Carnoy solution (6:3:1 ratio of 100% ethanol, chloroform, and glacial acetic acid), a nonaqueous fixative that preserves the secreted mucus layer, to the basolateral (1 mL) and apical (0.5 mL) compartments.[23] After 30 min of fixation at room temperature, inserts were washed twice with absolute methanol, twice with absolute ethanol, and twice with PBS. For blocking nonspecific background in all imaging experiments, inserts were incubated in 3% bovine serum albumin (BSA) in PBS, which was filter-sterilized, for 1 h at room temperature. The primary antibodies that were

used were mouse monoclonal anti-MU5AC (Santa Cruz, sc-21,701, 1:100) and mouse monoclonal anti-MUC5B (Santa Cruz, sc-21,768, 1:100). Primary antibody incubation was overnight at 4 °C in 1% BSA in PBS. After overnight incubation, inserts were washed with PBS twice and incubated in secondary antibody staining solution for 1 h at room temperature. The secondary antibody used was Donkey anti-Mouse IgG (H + L) Highly Cross-Adsorbed Secondary Antibody, Alexa Fluor 488 (Thermo Fisher Scientific, A-21202, RRID AB_141607). Inserts were washed with PBS twice and imaged at 10× magnification using a Zeiss Axio Observer and Axiocam 503 monocamera (Zeiss). For the nonprimary control, Donkey anti-Rabbit IgG (H + L) Highly Cross-Adsorbed Secondary Antibody, Alexa Fluor 647 (Thermo Fisher Scientific, catalog # A-31573, RRID AB_2536183) was used and background intensity was subtracted from anti-mucin images. MUC5B and MUC5AC staining was performed in separate BCi-NS1.1 cultures as the same species for the secondary antibody was used. Relative fluorescence intensities of MUC5B and MUC5AC in unstimulated and IL-13-stimulated cultures were quantified by normalizing the average fluorescence intensity of mucin staining to the percentage of fluorescence positive area. Quantification of mucin staining intensity and fluorescence positive area was performed with FIJI using the automated thresholding function.

2.8. Measurement of Mucus Transport and Ciliary Beat Frequency.

Mucociliary transport was measured based on the transport of 2 μm red-fluorescent polystyrene microspheres (Sigma-Aldrich). For measurement of the transport rate of native BCi-NS1.1 mucus, a 4 uL suspension of the fluorescent polystyrene microspheres (1:1000 dilution in PBS) was added on top of the native mucus, which was allowed to accumulate for 7 days. After 30 min of equilibration at 37 °C, videos of three regions were recorded at 10× magnification using a Zeiss 800 LSM microscope. Images were collected at a frame rate of 0.5 Hz for 10 s on the plane of the mucus gel. Images were acquired centrally within cultures and away from the edges where mucus tends to accumulate. For measurement of transport of synthetic mucus, BCi-NS1.1 native mucus was first removed from the cultures by washing the apical surfaces of cultures with PBS for 30 min. Forty microliters of the hydrogel was added to the apical surface (~40 μm thickness) of fully differentiated BCi-NS1.1 cells and equilibrated for 30 min at 37 °C. A suspension of 4 μL of 2 μm red-fluorescent polystyrene microspheres was added and allowed to equilibrate for an additional 30 min. For NAC experiments, fluorescent polystyrene microspheres were diluted in PBS containing 50 mM NAC in order to prevent further dilution of hydrogels. After 30 min of incubation, videos of at least three regions were recorded as described for the transport rates of BCi-NS1.1 native mucus. The microsphere tracking data analysis is based on an image processing algorithm that was custom-written in MATLAB (The MathWorks). Briefly, the analysis software computes the *xy*-plane trajectories of each fluorescent microsphere in each frame. Using the trajectory data, the displacement of microspheres was computed, and the transport rate was calculated by dividing the displacement of microsphere by the total time elapsed. In order to measure ciliary beat frequency (CBF), 10 s videos at a frame rate of 20 Hz were recorded at 10× magnification in ≥3 randomly selected regions of BCi-NS1.1 cultures using bright field. Using a custom-written algorithm in MATLAB, the number of local pixel intensity maxima was counted, which indicates beating of cilia. Beat frequency was determined by dividing the number of beats over the total elapsed time.

2.9. Measurement of Disulfide Bond Concentration in Synthetic Mucus.

Concentrations of disulfide bonds were measured using a previously described fluorometric assay.[22] Synthetic mucus hydrogels were resuspended in 8 M guanidine-HCl (Sigma) to 10 times the original hydrogel volume. In order to block free cysteines, samples were treated with 10% (v/v) 500 mM iodoacetamide for 1 h at room temperature. To quench excess iodoacetamide and reduce existing disulfide bonds, samples were treated with 10% (v/v) 1 M DTT at 37 °C. Samples were loaded into Amicon Ultra 10 kDa filters (Millipore-Sigma) and centrifuged at 14,000*g* for 20 min for removal of excess DTT and quenched iodoacetamide. Recovered samples were resuspended in 50 mM Tris–HCl (pH 8.0) and mixed with equal volumes of 2 mM monobromobimane (mBBr; Sigma). After 15 min of incubation in mBBr at room temperature, fluorescence was measured at 395 nm excitation/490 nm emission on a Spark Multimode Microplate reader (Tecan). Serial dilutions of 5 mM L-cysteine in 50 mM Tris–HCl were used as standards. Disulfide bond concentration was calculated against the standard curve.

2.10. Preparation of IAV and IAV Challenge Studies.

The plasmid-based reverse genetics system for influenza A virus (IAV) A/Puerto Rico/8/34 (PR8; H1N1) was a gift from Dr. Adolfo Garcia-Sastre. Infectious virus was generated from cloned cDNAs in 293 T and Madin-Darby canine kidney (MDCK) cell co-cultures and purified by ultracentrifugation through 20% sucrose onto a 50% sucrose cushion as previously described.[36] The infectivity of resulting virus stocks was quantified by the standard plaque assay on MDCK cells,[37] yielding a viral titer of 3.9×10^9 plaque-forming units (pfu)/mL. IAV was subsequently labeled with a lipophilic dye, 1,1′-dioctadecyl-3,3,3′3′-tetramethylindocarbocyanine perchlorate (DiI; Invitrogen). The labeled virions were then purified and concentrated via hemadsorption to chicken red blood cells.[37] IAV stock was aliquoted and stored at −80 °C. This strain exhibits a primarily spherical morphology and diameter of roughly 100 nm. DiI-labeled virus stocks were counterstained with an anti-H1N1 IAV HA antibody (NR-3148; antiserum, goat; BEI Resources, NIAID, NIH). Diffusion of IAV was assayed similarly to PTM studies. Mucin hydrogels were prepared in microscopy chambers, and 1 μL of DiI-labeled IAV was applied to the surface of the hydrogel and equilibrated for 30 min before imaging. The same tracking analysis employed in PTM experiments was used to compute the MSD of IAV. For experiments with IAV infection, BCi-NS1.1 cultures were initially washed with PBS to remove native mucus. Forty microliters of hydrogels with 75:25 and 25:75 MUC5B:MUC5AC ratios was added to the apical surface and allowed to equilibrate for 30 min. IAV (PR8) was then applied (4 μL; 7500 plaque-forming units (pfu)) centrally to HAE cultures and incubated for 2 h at 37 °C. After inoculation, cultures were rinsed with PBS prior to a 10 min wash at 37 °C to remove the hydrogel and nonabsorbed virus. Cultures were imaged 48 h after IAV, and hydrogels were removed. To image IAV infection, cultures were fixed in 1:1 methanol:acetone solution overnight at 4C. Afterward, cultures were washed in PBS and then permeabilized in 2.5% Triton X-100 for 15 min. After blocking, the primary antibody that was used was a mouse monoclonal anti-IAV nucleoprotein A1 and A3 blend (EMD Millipore, MAB8251, 1:250). Images were taken at 10× magnification using a Zeiss Axio Observer and Axiocam 503 mono camera (Zeiss). Percentages of infection area for uncoated and synthetic mucus coated cultures were determined by using the automated thresholding function in FIJI.

2.11. Statistical Analysis.

All graphing and statistical analyses were performed using GraphPad Prism 8 (GraphPad Software). Two-group comparisons were performed using 2-tailed Student's *t* test (normally distributed data) or Mann–Whitney *U* test. For comparisons between groups, one-way analysis of variance (ANOVA) followed by a Tukey post hoc correction was performed. Kruskal–Wallis with Dunn's correction was used for comparison of multiple groups with non-Gaussian distributions. Bar graphs show mean and standard deviation, box and whiskers plots show median values and 5th up to 95th percentiles of the data, and outliers were not included. Differences were considered statistically different at the level of $p < 0.05$.

3. RESULTS

3.1. Engineering Synthetic Mucus Biomaterials with Physicochemical Properties Similar to Human Mucus.

In this study, we aimed to create a synthetic mucus biomaterial with similar rheological and transport properties to human respiratory mucus. In our previous work, we reported the design of a hydrogel system that employs a thiol-based cross-linking strategy and verified that hydrogel assembly was mediated by hydrogen and disulfide bonding.[30] Using this approach, we prepared hydrogels with 2% (w/v) mucin and 2% (w/v) cross-linking reagent, PEG-4SH, using two types of mucins: porcine gastric mucin (PGM), containing MUC5AC,[38,39] and bovine submaxillary gland mucin (BSM), containing MUC5B (Figure 1A,B).[40,41] Given the limited volume (~50–100 μL) collected *ex vivo* from patients and generated *in vitro*, we chose to use particle tracking microrheology (PTM) to characterize the samples collected to compare to our synthetic model. Our results showed that MUC5B hydrogels had similar microrheology and pore network size to HAE-derived mucus, in the range of previously reported values (~200–300 nm).[24,25] Therefore, we used PTM to compare the physical properties of our synthetic mucus biomaterial to natural human airway mucus collected *ex vivo* from endotracheal tubes (ETTs) and *in vitro* collected from BCi-NS1.1 HAE cultures. Based on 100 nm PEG-NP diffusion, as measured by logarithm base 10 of mean squared displacement at a time lag of 1 s ($\log_{10}[MSD_{1s}]$), we find that *ex vivo* ETT mucus had similar microstructural properties to *in vitro* mucus samples derived from BCi-NS1.1 cultures.

Comparing our synthetic mucus biomaterials to human samples, we found that MUC5B (BSM) hydrogels had comparable microstructural properties to human mucus samples collected *in vitro* (Figure 1C). However, MUC5B hydrogels showed significantly different microstructural properties from ETT-sourced mucus (Figure 1C) as indicated by a reduction in 100 nm PEG-NP diffusion. The MUC5AC (PGM) gels had significantly reduced 100 nm PEG-NP diffusion compared to human mucus (*ex vivo* and *in vitro*) and MUC5B gels, indicative of a significantly smaller network pore size (Figure 1C). Using PTM analysis, we estimated the gel network pore sizes (ξ) in synthetic and human mucus. Similar to particle diffusion, MUC5B hydrogels showed similarities in pore size to the *in vitro* mucus samples ($\xi \approx$ 200–400 nm), whereas MUC5AC gels had significantly reduced network pore sizes ($\xi \approx$ 100 nm) (Figure 1D). We also observed varying distributions in nanoparticle diffusion and pore size in different samples, where MUC5AC hydrogels showed a smaller MSD and

pore size distribution than MUC5B hydrogels and human mucus samples. Based on the size of nanoparticles used (100 nm) for microrheological analysis, we are only able to detect network sizes ≥100 nm. Thus, MUC5AC hydrogels likely possess pore sizes of 100 nm or less.

Next, we measured and compared the transport rates of synthetic mucus and native mucus produced from BCi-NS1.1 HAE cultures. Although MUC5B hydrogels had similar microrheological properties to BCi-NS1.1 mucus, MUC5B gels showed significantly lower transport rates than native BCi-NS1.1 mucus. Alternatively, the MUC5AC hydrogel, which showed significantly reduced pore size, had significantly higher transport rates than MUC5B gels. Given that native mucus contains both MUC5B and MUC5AC, we prepared a hydrogel composed of a blend of both mucins with relative concentrations representative of healthy airway mucus. A previous study has shown that normal (nondiseased) human mucus is primarily composed of MUC5B (75–85%) and a smaller amount of MUC5AC (~15–25%).[19] To test whether a mixed ratio of mucins, specifically 75% MUC5B (BSM):25% MUC5AC (PGM), could mimic airway mucus, we measured the microrheological properties (Figure 1C,D) and transport rates (Figure 1E) of blended mucin hydrogels to compare to *ex vivo* and *in vitro* human mucus. Interestingly, we found that the blended gels had network sizes smaller than human samples based on PTM but had the most similar transport rate to the native mucus gels produced in BCi-NS1.1 HAE cultures.

3.2. Macro- and Microrheology of Synthetic Mucus with Varying MUC5B:MUC5AC Ratios.

Previous studies have demonstrated the relative increase in the abundance of MUC5AC compared to MUC5B in asthmatic mucus from adults and children where the percentage of MUC5AC reaches up to ~70% of the total mucin content.[19,42] Therefore, we sought to determine the effects of the mucin ratio, MUC5B:MU5AC, on the macro- and microrheological properties of synthetic mucus biomaterials. We systematically varied the MUC5B:MUC5AC ratio of starting hydrogels: (i) 75% MUC5B and 25% MUC5AC, representative of health, (ii) 50% MUC5B and 50% MUC5AC, representative of stable asthma, and (iii) 25% MUC5B and 75% MUC5AC, representative of exacerbated asthma.[19] For simplicity, we will refer to the 75:25 MUC5B:MUC5AC ratio as “MUC5B-rich” hydrogels and the 25:75 MUC5B:MUC5AC ratio as “MUC5AC-rich” hydrogels. We then compared the elastic moduli of mucin-based hydrogels at $\omega = 1$ rad/s, which revealed higher elastic and viscous moduli for hydrogels with higher MUC5AC content (Figure 2A,B). PTM analysis showed that a relative increase in MUC5AC content resulted in reduced particle diffusion, as measured by $\log_{10}[MSD_{1s}]$ of 100 nm PEG-NP, indicative of tightening of the mesh network of the hydrogels with increased MUC5AC content (Figure 2C). We also assessed diffusion of 500 nm PEG-NP as PEG-NP with a diameter greater than the pore size can probe physical properties closer to the bulk scale.[43] The diffusion of 500 nm PEG-NP showed a systematic reduction in $\log_{10}[MSD_{1s}]$ with increasing MUC5AC content, suggesting increased viscoelastic properties with increasing MUC5AC concentration (Figure 2D).

3.3. Measurement of Transport Rates of Synthetic Mucus with Varying MUC5B:MUC5AC Ratios.

Previous studies have shown that stimulation of primary HAE cultures with IL-13, a key mediator in asthma, results in increased MUC5AC production and markedly reduced mucus transport rates.[23,44] In order to establish and confirm asthmatic phenotype in our culture system, we stimulated BCi-NS1.1 HAE tissue cultures with IL-13 and performed *en face* staining to examine MUC5B and MUC5AC expression (Figure 3A). IL-13 stimulation in BCi-NS1.1 cultures consistently increased MUC5AC expression, whereas no significant changes were observed for MUC5B expression (Figure S2). We observed a significant reduction in transport rates of 2 μm microspheres in IL-13 stimulated cultures (Figure 3B,C). We also measured the cilia beat frequencies (CBFs) of BCi-NS1.1 cultures to confirm that the reduction of the transport rate was not due to changes in ciliary activity. We also confirmed that CBF was unaffected after IL-13 treatment (Figure 3D). We next sought to test whether mucin composition of synthetic mucus affects mucociliary transport rates by applying hydrogels with varying MUC5B:MUC5AC ratios on apically washed, mucus-free BCi-NS1.1 cultures. Based on microsphere trajectories, we found that the transport rates of MUC5AC-rich gels were significantly reduced in comparison to gels composed of equal MUC5B/MUC5AC concentrations or MUC5B-rich gels (Figure 3B,E). CBF was unaffected by the introduction of synthetic mucus with varied MUC5B:MUC5AC ratios (Figure 3F).

3.4. Impact of Disulfide Cross-Linking on the Transport of Asthma-like Synthetic Mucus Gels.

While a constant PEG-4SH concentration was used throughout our work, we hypothesized that enhanced viscoelasticity of MUC5AC-rich synthetic mucus may be a result of the higher number of available cysteines on MUC5AC noted in a previous study.[45] Therefore, we measured the disulfide bond concentration in hydrogels that showed significant differences in macro- and microrheological properties as well as transport rates for MUC5B-rich and MUC5AC-rich gels (Figure 4A). We found that the disulfide bond (S–S) concentration in MUC5AC-rich hydrogels was markedly higher than that in MUC5B-rich hydrogels. As enhanced elasticity resulting from increased disulfide cross-linking is considered a major factor in impairing mucus clearance,[22] we tested the effectiveness of *N*-acetylcysteine (NAC), a reducing agent that is used clinically as a mucolytic agent, in restoring transport rates of MUC5AC-rich gels on BCi-NS1.1 cultures. We observed that treatment with 50 mM NAC on MUC5AC-rich hydrogels significantly increased transport rates (Figure 4B), whereas CBF remained unchanged (Figure 4C). While MCC was improved with NAC treatment for the asthma-like MUC5AC-rich gels, transport rates were not restored to transport values of hydrogels composed of MUC5B-rich gels, representative of health (Figure 4B).

3.5. Barrier Properties of Asthma-like Synthetic Mucus Gels against Influenza A Viral Infection.

A previous study has shown that individuals with asthma are more susceptible to viral infections,[46] which can often cause an exacerbation of disease symptoms.[13] To determine if mucin composition could influence the barrier function of synthetic mucus toward influenza

A virus (IAV), we measured the diffusion rate of fluorescently labeled IAV in synthetic mucus with different MUC5B:MUC5AC ratios using PTM. We found that IAV had a higher average diffusion rate in MUC5AC-rich synthetic mucus than in MUC5B-rich gels (Figure 5A,B). However, the frequency distribution of $\log_{10}[MSD_{1s}]$ of individual IAV showed that only a small fraction of IAV could rapidly penetrate the MUC5B-rich (~7%) and MUC5AC-rich gels (~9%) (Figure 5C). We further tested if synthetic mucus with variable mucin content was more or less effective at blocking IAV infection in BCi-NS1.1 HAE cultures. In these studies, BCi-NS1.1 cultures were coated with MUC5B-rich (75:25) and MUC5AC-rich (25:75) synthetic mucus and challenged with 7500 pfu of IAV (multiplicity of infection ~0.15). IAV was introduced in minimal volume (4 μL) in order to avoid diluting mucus, and the inoculum was kept on the cultures for 2 h. Two days post infection, staining for IAV nucleoprotein revealed a significant reduction in successful infection by IAV when coated with MUC5B-rich synthetic mucus whereas MUC5AC-rich, asthma-like mucus had a similar amount of staining for IAV nucleoprotein to uncoated controls (Figure 5D,E).

4. DISCUSSION

In order to create synthetic mucus biomaterials with native-like function, we formulated mucin hydrogels using BSM, composed of MUC5B, and PGM, composed of MUC5AC, combined with a star PEG-thiol cross-linking agent to establish rheological properties similar to human airway mucus. We directly compared our synthetic mucus model to human mucus collected (i) from individuals without lung disease and (ii) from well-differentiated HAE tissue cultures. Although MUC5B gels were most similar to HAE-derived mucus, we observed significant differences between MUC5B gels and ETT-sourced mucus. We expect these differences to arise due to heterogeneity in microrheological properties in clinical samples of mucus as these samples possess high amounts of nonmucin biomolecules that can contribute to gel organization and microstructure.[26] MUC5AC hydrogels, on the other hand, had significantly smaller pore sizes (~100 nm) than “normal” *ex vivo* and *in vitro* human mucus that were comparable to previously reported properties of mucus in diseases, such as in CF.[21,25] To account for the potential effect mucin concentration and MW on the observed differences in hydrogel elasticity, we measured total protein content as well as hydrodynamic radii of mucin solutions. We found no significant differences between the protein concentrations and hydrodynamic sizes of MUC5B (BSM) and MUC5AC (PGM) solutions (Figure S1).

Due to the similarities in microrheological properties between MUC5B gels and HAE-derived mucus, we expected comparable transport rates on HAE cultures. Interestingly, transport rates of MUC5B gels were significantly lower than that of native HAE mucus (Figure 1), whereas MUC5AC gels exhibited significantly faster transport rates than MUC5B hydrogels despite differences in microrheological properties. Our results would suggest that MUC5B and MUC5AC gel transport could be influenced by factors other than network elasticity, such as friction or surface adhesion.[47,48] Of note, frictional coupling of the mucus gel to beating cilia can also contribute to its transport.[49] One would expect that more densely cross-linked gels will possess a higher degree of friction due to reduced water permeation at the gel–tissue interface. This may, in part, explain why the more highly cross-linked MUC5AC gels achieve faster transport rates than MUC5B gels due to an

enhanced coefficient of friction. However, additional studies are necessary to explore these potential effects on mucus transport. Overall, neither MUC5AC nor MUC5B hydrogels alone resembled both the biophysical and transport functions of native human mucus.

As native airway mucus is composed of both MUC5B and MUC5AC, we prepared hydrogels with both mucins at a physiological MUC5B:MUC5AC ratio of 75:25 (MUC5B-rich). Our results showed that blending of the mucins resulted in mucus clearance rates that were comparable to the transport of BCi-NS1.1 HAE mucus and also in the range of physiological values reported in the literature (~50 μm/s).[48] We should note that the bulk elastic moduli measured here, on the order of 200–400 Pa, are higher than previously reported moduli for human airway mucus (~10–50 Pa).[21,26,33] With the similarities in transport rates of synthetic and native human mucus on airway surfaces (Figure 1E), we expect that synthetic mucus is partially diluted, and as a result, its elasticity is reduced when equilibrated for 30 min on HAE tissue culture prior to experiments. Another limitation in our synthetic model is our use of nonhuman mucins, which possess species-specific differences in glycosylation. For example, BSM possesses similar terminal sialic acid groups to human MUC5B but also contains a small percentage of sialic acid glycoforms, such as *N*-glycolylneuraminic acid, not found in human tissues.[50] In addition, these mucins are only partially purified and contain other nonmucin components (e.g., albumin, immunoglobulin). However, mucin is the predominant polymeric component of our gels and, as such, likely dictates the mechanical and transport properties of these gels. In the airways, MUC5B and MUC5AC are known to be secreted in distinct cell types and reside in distinct regions of the epithelial surface.[51] As mucins are mixed homogeneously prior to gelation and application to HAE cells, it is unlikely our present model fully captures these effects. However, we have demonstrated that our synthetic mucus biomaterial exhibits transport rates in the range of physiological values in health and disease and thus provides a model system complementary to the *in vitro*, *ex vivo*, and *in vivo* models of mucociliary transport traditionally used.

Our results suggest that, independent of concentration, increases in MUC5AC, as observed in sputum samples from patients with asthma, could be sufficient to enhance the bulk viscoelastic properties of mucus (Figure 2). In the past, these changes in viscoelastic properties in asthma have been attributed to increased mucin concentration and excess plasma protein that may interfere with normal degradation and turnover of mucins in the airways.[21] While we presume that transport in IL-13-stimulated HAE will also be influenced by MUC5AC tethering to HAE as previously shown,[23] our data on synthetic mucus transport suggests that increasing MUC5AC in mucus gels may progressively slow MCC (Figure 3). We also found that the enhanced elasticity and reduced transport of MUC5AC-rich gels are likely due to increased disulfide cross-linking mediated by PEG-4SH (Figure 4). Given the importance of disulfide bonds in mucus gel elasticity, reducing agents such as *N*-acetylcysteine (NAC) have been used as an inhaled treatment to break down hyper-viscous mucus in chronic lung diseases like cystic fibrosis (CF) and chronic obstructive pulmonary disease (COPD).[52,53] Using NAC, we also found that reducing the disulfide bonds can significantly improve transport of asthma-like synthetic mucus with increased MUC5AC (Figure S3, Figure 4B).

Given the susceptibility to infection in those with underlying diseases like asthma,[12] we examined the role of the MUC5B:MUC5AC ratio in the barrier function of synthetic mucus toward IAV. We expected the tighter microstructure of MUC5AC-rich gels to reinforce barrier properties against IAV, restricting IAV diffusion. In contrast, we observed faster average diffusion of IAV in asthma-like, MUC5AC-rich gels than in MUC5B-rich gels (Figure 5B). However, in both MUC5B and MUC5AC-rich gels, we estimate that only a small fraction (7–9%) of IAV particles can diffuse rapidly enough to penetrate a ~40 μm mucus layer during the 2 h period of exposure to the viral inoculum used in our studies (Figure 5C). Given the similarities in IAV penetration, we expect that IAV diffusion within MUC5B-rich gels is influenced by mucin-associated glycan binding to a greater extent than the more heavily cross-linked MUC5AC-rich gels, which present a greater physical barrier to IAV diffusion. While these gel thicknesses and exposure times are more reflective of diseased airways, we note that thinner mucus layers and shorter clearance times (on the order of 30 min) would be expected in healthy lungs *in vivo*.[48] However, we kept gel thickness and inoculation time consistent for both MUC5B and MUC5AC-rich gels to enable direct comparisons. Notably, we found in HAE cultures challenged with IAV that the barrier properties of MUC5AC-rich gels toward IAV are significantly compromised, whereas MUC5B-rich gels are effective in neutralizing IAV (Figure 5D). It has been established in prior studies that IAV interacts with mucin glycans, primarily sialic acid.[54] In comparing mucin glycosylation profiles, MUC5B has been shown to contain a high concentration of sialic acid whereas MUC5AC contains greater fucose content.[3,18] Thus, we expect that the reduction in sialic acid content and transport rates of MUC5AC-rich gels could render the airway surface more susceptible to widespread and increased frequency of infection. We anticipate that the barrier properties of MUC5B-rich and MUC5AC-rich gels can be further understood by studying IAV diffusion through and the extent of infection in synthetic mucus-coated cultures using gels with modified glycosylated domains. Modification of mucin glycans, specifically removal of sialic acids, of BSM gels through enzymatic cleavage using sialidase has been demonstrated in prior work[55] and will be pursued in our future studies. In addition, prior work has demonstrated mucosal antibody-mediated trapping of IAV, which could also be explored using our synthetic model in the future.[56]

5. CONCLUSIONS

Our results establish a new biomaterial capable of recapitulating native airway mucus properties where mucus composition can be precisely controlled to study how its functions may be altered in diseases. Using bioengineered synthetic mucus, we have found that the changes observed in mucus composition in asthma can have a major impact on gel viscoelasticity, which in turn reduces its capacity to be effectively cleared. We also observed that asthma-like mucus biomaterials were less capable of protecting the airway surface from infection by IAV. To confirm the broader relevance of these findings to human diseases, future studies on mucus harvested *in vitro* from primary asthmatic tissue cultures and *ex vivo* isolated from patients with asthma will be performed to determine how rheology and barrier function toward respiratory viruses may be affected by changes in mucin composition. The model established herein could also be applied to other lung diseases

(e.g., COPD, CF, pulmonary fibrosis) to understand airway dysfunction and uncover disease mechanisms that provide the basis for new therapeutic interventions.

Supplementary Material

Refer to Web version on PubMed Central for supplementary material.

ACKNOWLEDGMENTS

This work was supported by the University of Maryland, Burroughs Wellcome Fund Career Award at the Scientific Interface (to G.A.D.), Parker B. Francis Fellowship in Pulmonary Research (to M.A.S.), Cystic Fibrosis Foundation (DUNCAN18I0 to G.A.D. and M.A.S.), and the NIH (R21AI142050 to M.A.S. and G.A.D., T32AI125186A to E.I.).

REFERENCES

(1). Dharmage SC; Perret JL; Custovic A.-n. Epidemiology of Asthma in Children and Adults. Front. Pediatr 2019, 7, 246. [PubMed: 31275909]

(2). Fanta CH Asthma. N. Engl. J. Med 2009, 360, 1002–1014. [PubMed: 19264689]

(3). Bonser L; Erle D Airway Mucus and Asthma: The Role of MUC5AC and MUC5B. J. Clin. Med 2017, 6, 112.

(4). Kesimer M; Ehre C; Burns KA; Davis CW; Sheehan JK; Pickles RJ Molecular Organization of the Mucins and Glycocalyx Underlying Mucus Transport over Mucosal Surfaces of the Airways. Mucosal Immunol. 2013, 6, 379–392. [PubMed: 22929560]

(5). Button B; Cai L-H; Ehre C; Kesimer M; Hill DB; Sheehan JK; Boucher RC; Rubinstein M A Periciliary Brush Promotes the Lung Health by Separating the Mucus Layer from Airway Epithelia. Science 2012, 337, 937–941. [PubMed: 22923574]

(6). Knowles MR; Boucher RC Mucus Clearance as a Primary Innate Defense Mechanism for Mammalian Airways. J. Clin. Invest 2002, 109, 571–577. [PubMed: 11877463]

(7). Dunican EM; Watchorn DC; Fahy JV Autopsy and Imaging Studies of Mucus in Asthma. Lessons Learned about Disease Mechanisms and the Role of Mucus in Airflow Obstruction. Ann. Am. Thorac. Soc 2018, 15, S184–S191. [PubMed: 30431352]

(8). Fahy JV; Dickey BF Airway Mucus Function and Dysfunction. N. Engl. J. Med 2010, 363, 2233–2247. [PubMed: 21121836]

(9). Kuyper LM; Paré PD; Hogg JC; Lambert RK; Ionescu D; Woods R; Bai TR Characterization of Airway Plugging in Fatal Asthma. Am. J. Med 2003, 115, 6–11. [PubMed: 12867228]

(10). Teach SJ; Crain EF; Quint DM; Hylan ML; Joseph JG Improved Asthma Outcomes in a High-Morbidity Pediatric Population. Arch. Pediatr. Adolesc. Med 2006, 160, 535. [PubMed: 16651498]

(11). Dougherty RH; Fahy JV Acute Exacerbations of Asthma: Epidemiology, Biology and the Exacerbation-Prone Phenotype. Clin. Exp. Allergy 2009, 39, 193–202. [PubMed: 19187331]

(12). Mallia P; Johnston SL How Viral Infections Cause Exacerbation of Airway Diseases. Chest 2006, 130, 1203–1210. [PubMed: 17035457]

(13). Busse WW; Lemanske RF Jr.; Gern JE Role of Viral Respiratory Infections in Asthma and Asthma Exacerbations. Lancet 2010, 376, 826–834. [PubMed: 20816549]

(14). Boucher RC On the Pathogenesis of Acute Exacerbations of Mucoobstructive Lung Diseases. Ann. Am. Thorac. Soc 2015, 12 Suppl 2, S160–S163. [PubMed: 26595733]

(15). Song D; Cahn D; Duncan GA Mucin Biopolymers and Their Barrier Function at Airway Surfaces. Langmuir 2020, 12773. [PubMed: 33094612]

(16). Samad T; Co JY; Witten J; Ribbeck K Mucus and Mucin Environments Reduce the Efficacy of Polymyxin and Fluoroquinolone Antibiotics against *Pseudomonas Aeruginosa*. ACS Biomater. Sci. Eng 2019, 5, 1189–1194. [PubMed: 33405639]

(17). Sheehan JK; Brazeau C; Kutay S; Pigeon H; Kirkham S; Howard M; Thornton DJ Physical Characterization of the MUC5AC Mucin: A Highly Oligomeric Glycoprotein Whether Isolated from Cell Culture or in Vivo from Respiratory Mucous Secretions. Biochem. J 2000, 347, 37–44. [PubMed: 10727399]

(18). Raclawska DS; Ttofali F; Fletcher AA; Harper DN; Bochner BS; Janssen WJ; Evans CM Mucins and Their Sugars. Critical Mediators of Hyperreactivity and Inflammation. Ann. Am. Thorac. Soc 2016, 13 Suppl 1, S98–S99.

(19). Lachowicz-Scroggins ME; Yuan S; Kerr SC; Dunican EM; Yu M; Carrington SD; Fahy JV Abnormalities in MUC5AC and MUC5B Protein in Airway Mucus in Asthma. Am. J. Respir. Crit. Care Med 2016, 194, 1296–1299. [PubMed: 27845589]

(20). Dunican EM; Elicker BM; Gierada DS; Nagle SK; Schiebler ML; Newell JD; Raymond WW; Lachowicz-Scroggins ME; Di Maio S; Hoffman EA; Castro M; Fain SB; Jarjour NN; Israel E; Levy BD; Erzurum SC; Wenzel SE; Meyers DA; Bleecker ER; Phillips BR; Mauger DT; Gordon ED; Woodruff PG; Peters MC; Fahy JV; Noel P; Smith R; The National Heart Lung and Blood Institute (NHLBI) Severe Asthma Research Program (SARP). Mucus Plugs in Patients with Asthma Linked to Eosinophilia and Airflow Obstruction. J. Clin. Invest 2018, 128, 997–1009. [PubMed: 29400693]

(21). Innes AL; Carrington SD; Thornton DJ; Kirkham S; Rousseau K; Dougherty RH; Raymond WW; Caughey GH; Muller SJ; Fahy JV *Ex Vivo* Sputum Analysis Reveals Impairment of Protease-Dependent Mucus Degradation by Plasma Proteins in Acute Asthma. Am. J. Respir. Crit. Care Med 2009, 180, 203–210. [PubMed: 19423716]

(22). Yuan S; Hollinger M; Lachowicz-Scroggins ME; Kerr SC; Dunican EM; Daniel BM; Ghosh S; Erzurum SC; Willard B; Hazen SL; Huang X; Carrington SD; Oscarson S; Fahy JV Oxidation Increases Mucin Polymer Cross-Links to Stiffen Airway Mucus Gels. Sci. Transl. Med 2015, 7, 276ra27–276ra27.

(23). Bonser LR; Zlock L; Finkbeiner W; Erle DJ Epithelial Tethering of MUC5AC-Rich Mucus Impairs Mucociliary Transport in Asthma. J. Clin. Invest 2016, 126, 2367–2371. [PubMed: 27183390]

(24). Schuster BS; Suk JS; Woodworth GF; Hanes J Nanoparticle Diffusion in Respiratory Mucus from Humans without Lung Disease. Biomaterials 2013, 34, 3439–3446. [PubMed: 23384790]

(25). Duncan GA; Jung J; Joseph A; Thaxton AL; West NE; Boyle MP; Hanes J; Suk JS Microstructural Alterations of Sputum in Cystic Fibrosis Lung Disease. JCI insight 2016, 1, No. e88198. [PubMed: 27812540]

(26). Markovetz MR; Subramani DB; Kissner WJ; Morrison CB; Garbarine IC; Ghio A; Ramsey KA; Arora H; Kumar P; Nix DB; Kumagai T; Krunkosky TM; Krause DC; Radicioni G; Alexis NE; Kesimer M; Tiemeyer M; Boucher RC; Ehre C; Hill DB Endotracheal Tube Mucus as a Source of Airway Mucus for Rheological Study. Am. J. Physiol.-Lung Cell. Mol Physiol 2019, 317, L498–L509. [PubMed: 31389736]

(27). Sears PR; Yin W-N; Ostrowski LE Continuous Mucociliary Transport by Primary Human Airway Epithelial Cells in Vitro. Am. J. Physiol.-Lung Cell. Mol. Physiol 2015, 309, L99–L108. [PubMed: 25979076]

(28). Celli JP; Turner BS; Afdhal NH; Ewoldt RH; McKinley GH; Bansil R; Erramilli S Rheology of Gastric Mucin Exhibits a PH-Dependent Sol-Gel Transition. Biomacromolecules 2007, 8, 1580–1586. [PubMed: 17402780]

(29). Huck BC; Hartwig O; Biehl A; Schwarzkopf K; Wagner C; Loretz B; Murgia X; Lehr C-M Macro- And Microrheological Properties of Mucus Surrogates in Comparison to Native Intestinal and Pulmonary Mucus. Biomacromolecules 2019, 20, 3504–3512. [PubMed: 31419118]

(30). Joyner K; Song D; Hawkins RF; Silcott RD; Duncan GA A Rational Approach to Form Disulfide Linked Mucin Hydrogels. Soft Matter 2019, 9632. [PubMed: 31651920]

(31). Schuster BS; Ensign LM; Allan DB; Suk JS; Hanes J Particle Tracking in Drug and Gene Delivery Research: State-of-the-Art Applications and Methods. Adv. Drug Delivery Rev 2015, 91, 70–91.

(32). Walters MS; Gomi K; Ashbridge B; Moore MAS; Arbelaez V; Heldrich J; Ding B-S; Rafii S; Staudt MR; Crystal RG Generation of a Human Airway Epithelium Derived Basal Cell Line with Multipotent Differentiation Capacity. Respir. Res 2013, 14, 135. [PubMed: 24298994]

(33). Hill DB; Vasquez PA; Mellnik J; McKinley SA; Vose A; Mu F; Henderson AG; Donaldson SH; Alexis NE; Boucher RC; Forest MG A Biophysical Basis for Mucus Solids Concentration as a Candidate Biomarker for Airways Disease. PLoS One 2014, 9, No. e87681. [PubMed: 24558372]

(34). Hill DB; Button B Establishment of Respiratory Air-Liquid Interface Cultures and Their Use in Studying Mucin Production, Secretion, and Function. Methods Mol. Biol 2012, 842, 245–258. [PubMed: 22259141]

(35). Kesimer M; Ford AA; Ceppe A; Radicioni G; Cao R; Davis CW; Doerschuk CM; Alexis NE; Anderson WH; Henderson AG; Barr RG; Bleecker ER; Christenson SA; Cooper CB; Han MK; Hansel NN; Hastie AT; Hoffman EA; Kanner RE; Martinez F; Paine R III; Woodruff PG; O'Neal WK; Boucher RC Airway Mucin Concentration as a Marker of Chronic Bronchitis. N. Engl. J. Med 2017, 377, 911–922. [PubMed: 28877023]

(36). Lugovtsev VY; Melnyk D; Weir JP Heterogeneity of the MDCK Cell Line and Its Applicability for Influenza Virus Research. PLoS One 2013, 8, No. e75014. [PubMed: 24058646]

(37). Hutchinson EC; Charles PD; Hester SS; Thomas B; Trudgian D; Martínez-Alonso M; Fodor E Conserved and Host-Specific Features of Influenza Virion Architecture. Nat. Commun 2014, 5, 4816. [PubMed: 25226414]

(38). Schömig VJ; Käsdorf BT; Scholz C; Bidmon K; Lieleg O; Berensmeier S An Optimized Purification Process for Porcine Gastric Mucin with Preservation of Its Native Functional Properties. RSC Adv. 2016, 6, 44932–44943.

(39). Stürmer R; Harder S; Schlüter H; Hoffmann W Commercial Porcine Gastric Mucin Preparations, Also Used as Artificial Saliva, Are a Rich Source for the Lectin TFF2: In Vitro Binding Studies. ChemBioChem 2018, 19, 2598–2608. [PubMed: 30371971]

(40). Carvalho SB; Moreira AS; Gomes J; Carrondo MJT; Thornton DJ; Alves PM; Costa J; Peixoto C A Detection and Quantification Label-Free Tool to Speed up Downstream Processing of Model Mucins. PLoS One 2018, 13, No. e0190974. [PubMed: 29315346]

(41). Jiang W; Gupta D; Gallagher D; Davis S; Bhavanandan VP The Central Domain of Bovine Submaxillary Mucin Consists of over 50 Tandem Repeats of 329 Amino Acids: Chromosomal Localization of the *BSM1* Gene and Relations to Ovine and Porcine Counterparts. Eur. J. Biochem 2000, 267, 2208–2217. [PubMed: 10759843]

(42). Welsh KG; Rousseau K; Fisher G; Bonser LR; Bradding P; Brightling CE; Thornton DJ; Gaillard EA MUC5AC and a Glycosylated Variant of MUC5B Alter Mucin Composition in Children With Acute Asthma. Chest 2017, 152, 771–779. [PubMed: 28716644]

(43). Lai SK; Wang Y-Y; Wirtz D; Hanes J Micro- and Macrorheology of Mucus. Adv. Drug Delivery Rev 2009, 61, 86–100.

(44). Koh KD; Siddiqui S; Cheng D; Bonser LR; Sun DI; Zlock LT; Finkbeiner WE; Woodruff PG; Erle DJ Efficient RNP-Directed Human Gene Targeting Reveals SPDEF Is Required for IL-13-Induced Mucostasis. Am. J. Respir. Cell Mol. Biol 2020, 62, 373–381. [PubMed: 31596609]

(45). Thornton DJ; Rousseau K; McGuckin MA Structure and Function of the Polymeric Mucins in Airways Mucus. Annu. Rev. Physiol 2008, 70, 459–486. [PubMed: 17850213]

(46). Veerapandian R; Snyder JD; Samarasinghe AE Influenza in Asthmatics: For Better or for Worse? Front. Immunol 2018, 9, 1843. [PubMed: 30147697]

(47). Button B; Goodell HP; Atieh E; Chen Y-C; Williams R; Shenoy S; Lackey E; Shenkute NT; Cai L-H; Dennis RG; Boucher RC; Rubinstein M Roles of Mucus Adhesion and Cohesion in Cough Clearance. Proc. Natl. Acad. Sci 2018, 115, 12501–12506. [PubMed: 30420506]

(48). Boucher RC Muco-Obstructive Lung Diseases. N. Engl. J. Med 2019, 380, 1941–1953. [PubMed: 31091375]

(49). Matsui H; Randell SH; Peretti SW; Davis CW; Boucher RC Coordinated Clearance of Periciliary Liquid and Mucus from Airway Surfaces. J. Clin. Invest 1998, 102, 1125–1131. [PubMed: 9739046]

(50). Kim J; Ryu C; Ha J; Lee J; Kim D; Ji M; Park CS; Lee J; Kim DK; Kim HH Structural and Quantitative Characterization of Mucin-Type O-Glycans and the Identification of OGlycosylation Sites in Bovine Submaxillary Mucin. Biomolecules 2020, 10, 636.

(51). Ostedgaard LS; Moninger TO; McMenimen JD; Sawin NM; Parker CP; Thornell IM; Powers LS; Gansemer ND; Bouzek DC; Cook DP; Meyerholz DK; Alaiwa MHA; Stoltz DA; Welsh MJ

Gel-Forming Mucins Form Distinct Morphologic Structures in Airways. Proc. Natl. Acad. Sci 2017, 114, 6842–6847. [PubMed: 28607090]

(52). Ehre C; Rushton ZL; Wang B; Hothem LN; Morrison CB; Fontana NC; Markovetz MR; Delion MF; Kato T; Villalon D; Thelin WR; Esther CR Jr.; Hill DB; Grubb BR; Livraghi-Butrico A; Donaldson SH; Boucher RC An Improved Inhaled Mucolytic to Treat Airway Muco-Obstructive Diseases. Am. J. Respir. Crit. Care Med 2019, 199, 171–180. [PubMed: 30212240]

(53). Hancock LA; Hennessy CE; Solomon GM; Dobrinskikh E; Estrella A; Hara N; Hill DB; Kissner WJ; Markovetz MR; Grove Villalon DE; Voss ME; Tearney GJ; Carroll KS; Shi Y; Schwarz MI; Thelin WR; Rowe SM; Yang IV; Evans CM; Schwartz DA Muc5b Overexpression Causes Mucociliary Dysfunction and Enhances Lung Fibrosis in Mice. Nat. Commun 2018, 9, 5363. [PubMed: 30560893]

(54). de Vries E; Du W; Guo H; de Haan CAM Influenza A Virus Hemagglutinin–Neuraminidase–Receptor Balance: Preserving Virus Motility. Trends Microbiol. 2020, 28, 57–67. [PubMed: 31629602]

(55). Yan H; Hjorth M; Winkeljann B; Dobryden I; Lieleg O; Crouzier T Glyco-Modification of Mucin Hydrogels to Investigate Their Immune Activity. ACS Appl. Mater. Interfaces 2020, 12, 19324–19336. [PubMed: 32301325]

(56). Wang Y-Y; Harit D; Subramani DB; Arora H; Kumar PA; Lai SK Influenza-Binding Antibodies Immobilise Influenza Viruses in Fresh Human Airway Mucus. Eur. Respir. J 2017, 49, 1601709. [PubMed: 28122865]

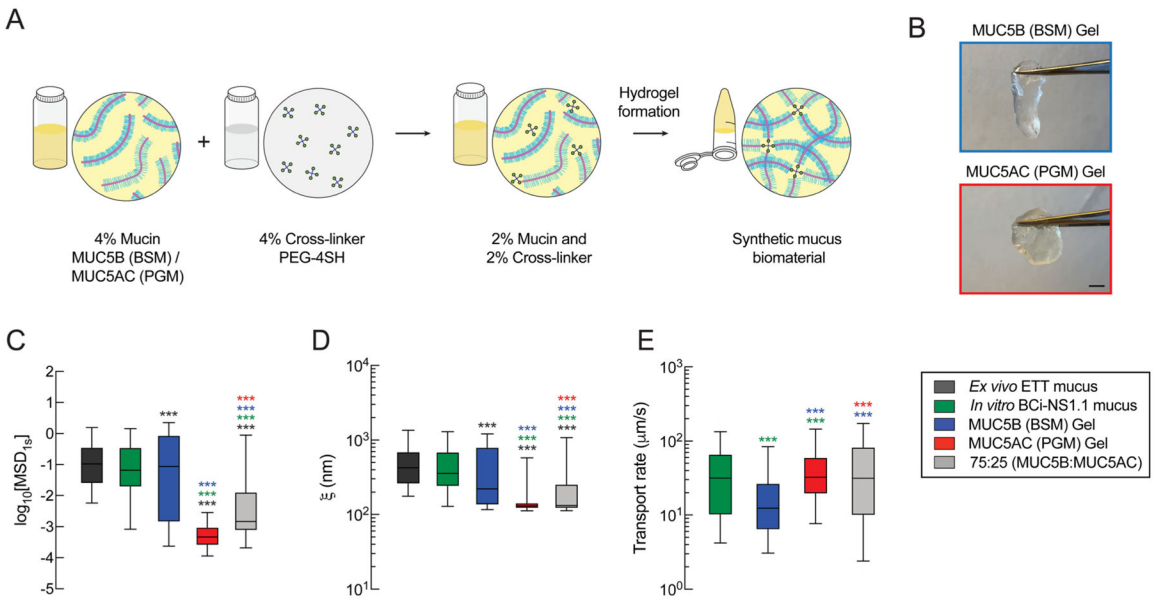

Figure 1.

Comparison of the biophysical and transport properties of native human mucus to synthetic mucus biomaterials. (A) Schematic illustration of the preparation steps for the synthetic mucus biomaterial. 4% (w/v) mucin solution is mixed with a 4% (w/v) cross-linker to form a mucin-based hydrogel with 2% (w/v) mucin and 2% (w/v) cross-linker. (B) Images of MUC5B (BSM) hydrogel (blue) and MUC5AC (PGM) hydrogels (red). Scale bar = 2 mm. (C) Box-and-whisker plots of measured $\log_{10}[MSD_{1s}]$ for 100 nm PEG-NP in human mucus samples (*ex vivo* and *in vitro*) and synthetic mucus biomaterials with varying mucin compositions. (D) Box-and-whisker plots of the estimated pore sizes (ξ) of human mucus samples and synthetic mucus biomaterials calculated based on 100 nm PEG-NP diffusion. (E) Box-and-whisker plots of the microsphere transport rates of BCi-NS1.1 native mucus and synthetic mucus biomaterials on BCi-NS1.1 cultures.***$p < 0.001$ by Kruskal–Wallis test with Dunn's correction. The color of the asterisk indicates the comparison group.

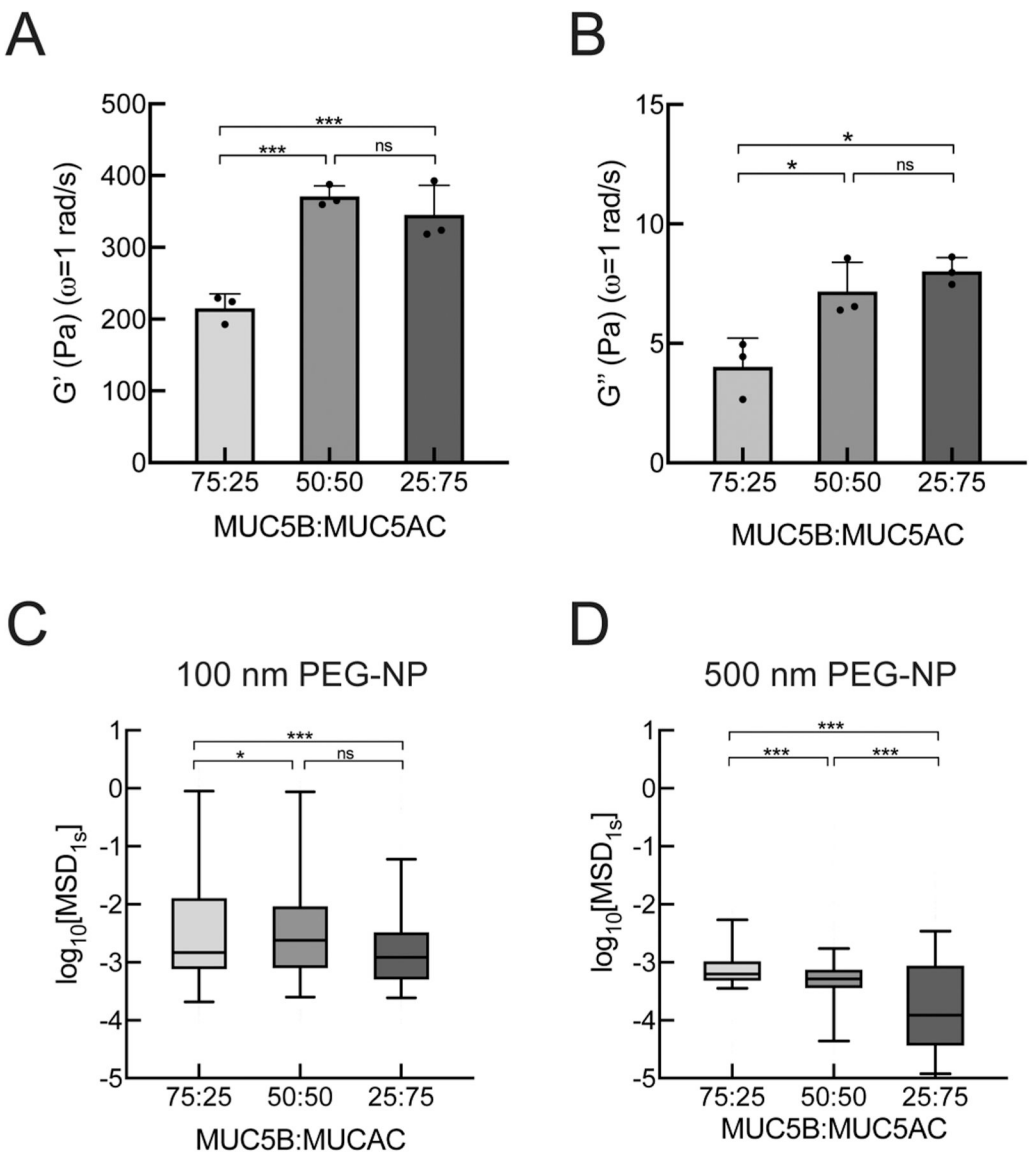

Figure 2.

Macro- and microrheology of synthetic mucus with varied concentrations of MUC5B and MUC5AC. (A) Mean elastic and (B) viscous moduli (G', G'') of hydrogels with varying MUC5B:MU5AC ratios at $\omega = 1$ rad/s measured using bulk rheology. (C) Box-and-whisker plots of measured $\log_{10}[MSD_{1s}]$ for 100 nm PEG-NP in hydrogels with varying MUC5B:MU5AC ratios. (D) Box-and-whisker plots of measured $\log_{10}[MSD_{1s}]$ for 500 nm PEG-NP in hydrogels with varying MUC5B:MU5AC ratios. ***$p < 0.001$, *$p < 0.05$ by (A,B) one-way ANOVA and (C,D) by Kruskal–Wallis test with Dunn's correction.

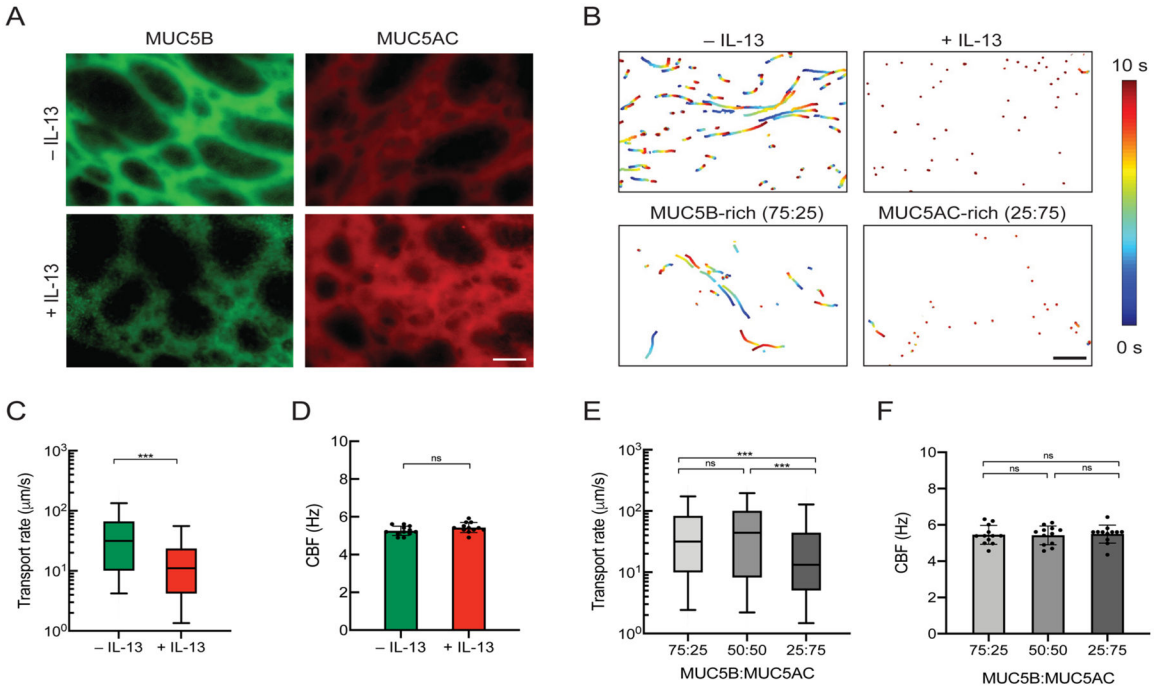

Figure 3.

Mucociliary transport in human airway epithelial (HAE) cultures for native mucus in IL-13-stimulated HAE and synthetic mucus with varied MUC5B:MUC5AC ratios. (A) *En face* immunostaining of mucus gels produced from unstimulated (−IL-13) or IL-13-stimulated (+IL-13) BCi-NS1.1 HAE cultures. Scale bar = 20 μm. (B) Paths of fluorescent microspheres deposited onto gels from −IL-13 and +IL-13 BCi-NS1.1 cultures and synthetic mucus gels (shown conditions are MUC5B-rich (75:25) and MUC5AC-rich (25:75) gels). Trajectories show 10 s of motion with a color scale that indicates time elapsed. Scale bar = 100 μm. (C) Box-and-whisker plots of the microsphere transport rates on −IL-13 and +IL-13 BCi-NS1.1 cultures. ***$p < 0.001$ by Mann–Whitney U test. (D) Mean ciliary beat frequencies of −IL-13 and +IL-13 BCi-NS1.1 cultures. (E) Box-and-whisker plots of the microsphere transport rates on BCi-NS1.1 cultures with hydrogels with varying MUC5B:MUC5AC ratios. ***$p < 0.001$ by Kruskal–Wallis test with Dunn's correction. (F) Mean ciliary beat frequencies of BCi-NS1.1 cultures with hydrogels with varying MUC5B:MUC5AC ratios.

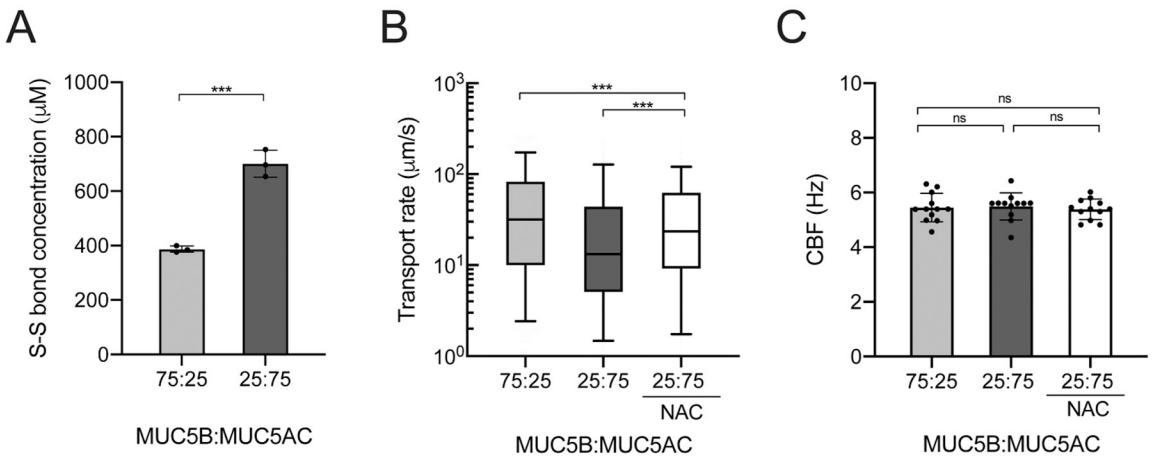

Figure 4.

Influence of disulfide cross-linking on asthma-like synthetic mucus transport function. (A) Mean disulfide bond (S–S) concentrations in MUC5B-rich (75:25) and MUC5AC-rich (25:75) gels. ***$p < 0.001$ by unpaired Student's t test. (B) Box-and-whisker plots of the microsphere transport rates on BCi-NS1.1 HAE cultures with MUC5B-rich (75:25) and MUC5AC-rich (25:75) hydrogels and MUC5AC-rich hydrogel (25:75) with NAC treatment. ***$p < 0.001$ by Kruskal–Wallis test with Dunn's correction. (C) Ciliary beat frequencies of BCi-NS1.1 HAE cultures.

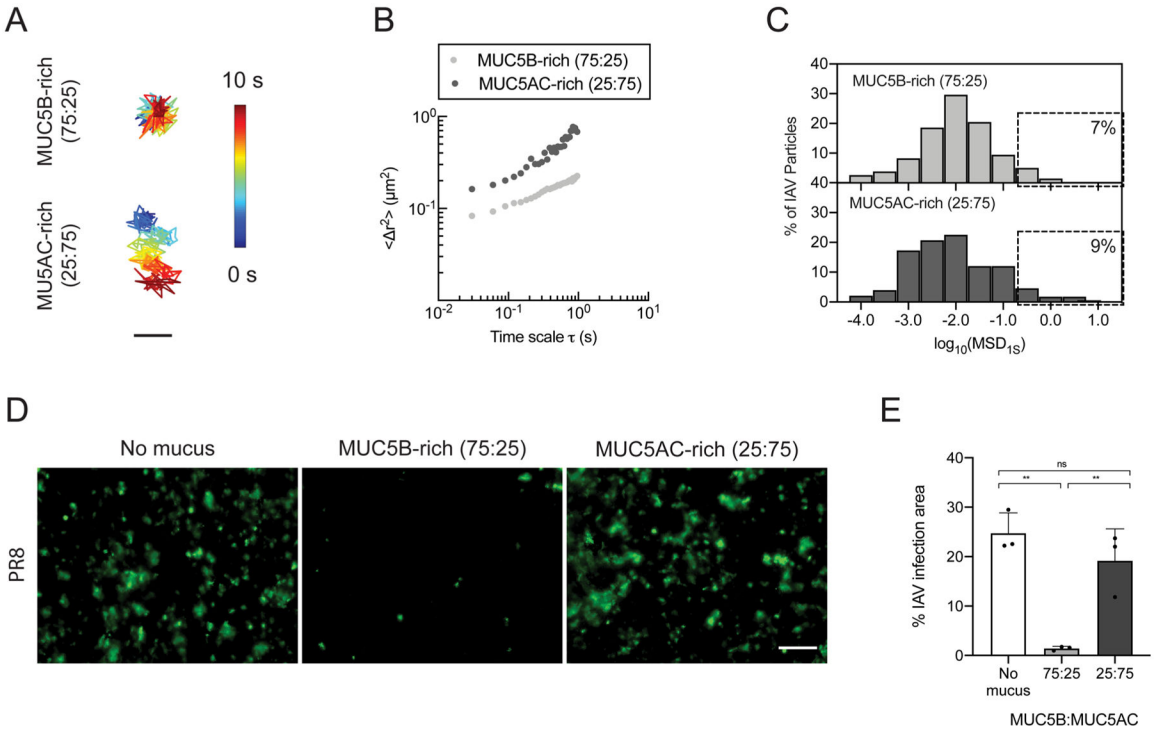

Figure 5.

Barrier function of normal and asthma-like synthetic mucus toward influenza A virus (IAV). (A) Trajectories of IAV diffusion in MUC5B-rich (75:25) and MUC5AC-rich (25:75) gels. Trajectories show 10 s of motion with a color scale that indicates time elapsed. Scale bar = 200 nm. (B) Ensemble average MSDs ($\langle \Delta r^2 \rangle$) of DiI-labeled IAV as a function of time scale (τ) in MUC5B-rich (75:25) and MUC5AC-rich (25:75) gels. (C) Frequency distributions of $\log_{10}[MSD_{1s}]$ of individual IAV in MUC5B-rich (75:25) and MUC5AC-rich gels (25:75). (D) Fluorescence micrographs of uncoated and synthetic mucus-coated BCi-NS1.1 cultures infected apically with IAV (PR8) 48 hpi after 2 h of inoculation. Green indicates staining for IAV nucleoprotein. Scale bar = 20 μm. (E) Percentages of infection area as determined by IAV nucleoprotein staining for uncoated and synthetic mucus-coated BCi-NS1.1 cultures.